The Effect of Substrate Material on Silver Nanoparticle Antimicrobial Efficacy

Benita J. Dair [1,*], David M. Saylor [1], T. Eric Cargal [1], Grace R. French [1], Kristen M. Kennedy [1], Rachel S. Casas [1], Jonathan E. Guyer [2], James A. Warren [2], and Steven K. Pollack [1]

1 FDA Center for Devices and Radiological Health, Office of Science and Engineering Labs, Division of Chemistry and Materials Science, Silver Spring, MD
2 National Institute of Standards and Technology, Gaithersburg, MD
* Contact Information: benita.dair@fda.hhs.gov

Abstract

With the advent of nanotechnology, silver nanoparticles increasingly are being used in coatings, especially in medical device applications, to capitalize on their antimicrobial properties. The increased antimicrobial efficacy of nanoparticulate silver systems relative to their bulk counterparts may be attributed to an increased silver ion (Ag^+) solubility, and hence availability, that arises due to large curvatures of the small nanometer-sized particles. However, a change of the material upon which the antimicrobial nanoparticulate silver is deposited (herein called "substrate") may affect the availability of Ag^+ ions and the intended efficacy of the device. We utilize both theory and experiment to determine the effect of substrate on ion release from silver particles in electrochemical environments and find that substrate surface charge, chemical reactivity or affinity of the surface for Ag^+ ions, and wettability of the surface all affect availability of Ag^+ ions, and hence antimicrobial efficacy. It is also observed that with time of

exposure to DI water, Ag+ ion release increases to a maximum value at 5 minutes before decreasing to undetectable levels, which is attributed to coarsening of the nanoparticles, which subsequently reduces the solubility and availability of Ag+ ions. This coarsening phenomenon is also predicted by the theoretical considerations and has been confirmed experimentally by TEM.

Introduction

Silver has long been known to have antimicrobial properties, as far back as ancient times, and were used until chemical antibiotics came into vogue [1-3]. However, with the advent of nanotechnology, silver is re-emerging as an antimicrobial, especially in medical device and consumer products applications [3]. Although in bacteria the mechanisms of silver activity are not completely known, it is thought that the Ag^{+} ions are the active species that disrupts critical cell functions and is hence the source of antimicrobial activity while metallic silver is inert [4-10]. In a silver particle, only atoms at the surface exposed to an aqueous environment are oxidized to take on ionic form (Ag^{+}). Decreasing the size of silver particles to the nanoscale regime increases particle curvature and hence the silver ion solubility in solution, thereby enhancing their potential antimicrobial efficacy relative to their bulk counterparts. Previously termed “colloidal silver”, nanoparticulate silver has been used in the medical community as antimicrobial agents for medical device applications, such as bandages, wound dressings, surgical masks, endotracheal tubes, and catheters [1-3].

In the case of device materials, a change of the material upon which the antimicrobial nanoparticulate silver is deposited (herein called “substrate”) may affect the intended efficacy of the device. As most of the medical devices with nanoparticulate silver are exposed to biological environments containing ionic species, such as Na^{+}, Ca^{2+}, Cl^{-}, PO^{4-}, etc., we use both theory and

experiment to determine the effect of the substrate on ion release from silver nanoparticles in electrochemical environments.

Experimental

Silver nanoparticles were synthesized according to the method of Lee and Meisel [11]. Silver nitrate ($1x10^{-1}$ mol/L) and sodium citrate powder (Aldrich Chemical Co.) were diluted to a $1x10^{-3}$ mol/L silver nitrate solution and an aqueous 1 % mass fraction sodium citrate solution respectively, using 18 MΩ-cm water filtered and deionized using a Barnstead NANOpure DIamond deionization system [12].

In a glass container 50 mL of 1 x 10^{-3} mol/L silver nitrate was heated with stirring to boiling, at which point 2 mL of the sodium citrate solution was then added. When a color change was noted, the solution was subsequently removed from heat and quenched with stirring in an ice bath. Nanoparticle size and zeta potential were characterized by a Malvern Zetasizer dynamic light scattering instrument to be 5 nm to 10 nm by volume distribution and -35 mV, respectively. Silver solution was deposited onto lacey carbon-coated Cu grids and the morphologies of the particles were observed with a JEOL 100CX Transmission Electron Microscope, operated at 80 kV.

Surfaces of various sheets of materials representative of relevant medical devices were were prepared for testing by soaking and washing first in ethanol, then in water, and dried in ambient conditions under cover. Ten microliter droplets of the silver nanoparticle solutions were deposited on the surfaces and allowed to dry covered, simulating a medical device coating process.

Much data indicate that metallic silver, or Ag^0, is inert, but that the Ag^+ ion is the active species in antimicrobial activity [3-8]. Therefore, the concentration of Ag^+ in local solution as determined by the ion selective electrode is used as a surrogate measure of antimicrobial effectiveness. Droplets were re-wet using ten microliters of deionized (DI) water to simulate a medical device in use. Silver ion (Ag^+) concentrations were measured using an Orion 94-16 silver/sulfide ion selective electrode with an Orion 4 Star Portable meter.

Computational

To predict the electrochemical response of the metallic nanoparticles, such as Ag, we have developed a multi-phase field electrochemical model. The model is formulated by building upon concepts previously described by Guyer *et al.* (electrochemistry) [13-14] and Rappaz *et al.* (multi-phase) [15]. We consider a system consisting of metallic particles in ionic solution described by five ionic components: electrons e^- and cations M^+, of which the particles are primarily comprised, and a neutral solvent S^0 containing a dissociated salt, N^+ and A^-. The composition variations within the system are expressed by the molar concentration of these components, C_i. Further, we introduce a series of phase parameters, ξ_j, that describe physical variations throughout the system including transitions between the liquid solution and solid particles as well as transitions in crystalline orientation between particles. Here, we employ five phase parameters: four different solid orientations and the liquid phase. Finally, we also consider fluctuations in the electrostatic potential, ϕ, throughout the system.

Based on these parameters, we postulate the following form for the free energy in our model:

$$F(C_i,\xi_j,\phi)=\int_V dV\left[f(C_i,\xi_L)+\sum_{j,k>j}\left(W\xi_j^2\xi_k^2+\frac{\alpha}{2}|\xi_j\nabla\xi_k-\xi_k\nabla\xi_j|^2\right)+\frac{\rho\phi}{2}\right]. \quad (1)$$

The first term in Eqn. 1 contains the bulk (homogeneous) contributions to the free energy, which is a function of composition and whether the components are in the solid or liquid phase, denoted by the liquid phase parameter, ξ_L, which varies between zero (solid) and one (liquid). We set $f(C_i,\xi_L)=\sum_i C_i\left[\Delta\mu_i^{\circ}(1-p(\xi_L))+RT\ln C_i V_m\right]$, where $\Delta\mu_i^{\circ}$ are the free energy differences between the solid and liquid phase for the pure components, $p(\xi_L)$ is an interpolating function, V_m is the molar volume, R is the gas constant, and T is the prescribed temperature. The terms inside the summation represent the interfacial contributions to the free energy with coefficients, W and α, related to the energy and thickness of non-electrified interfaces between the pure components. The final term contains the electrical contributions to the energy with charge density $\rho=F\sum_i z_i C_i$, where z_i are the component valences and $\mathcal{F}$ is Faraday's constant.

Based on the above form for the free energy, a standard variational analysis is performed to specify the equations that govern the evolution of the field variables that describe the system. These equations are postulated as the simplest time-dependent forms that guarantee a decrease in the total free energy with time while ensuring conservation of species. For brevity, the details of their derivation are omitted here. We note, however, that the electrons are treated as an interstitial species with zero partial molar volume ($V_{e^-}=0$), while the remaining components are substitutional with identical partial volumes V_s. This treatment results in four independent partial differential equations that describe the evolution of the concentration fields, which can be specified as

$$\frac{\partial C_i}{\partial t} = \nabla \cdot M_i \nabla \left[\frac{\delta F}{\delta C_i} - \frac{V_i}{V_s} \frac{\delta F}{\delta C_{S^0}} \right], \quad (2)$$

for $i \neq S^0$ with $M_i = D(1+V_s C_{e^-})C_{e^-}$ for $i = e^-$ and $M_i = Dp(\xi_L)C_i C_{S^0} / RT(C_i + C_{S^0})$ otherwise. Further, we specify four independent partial differential equations that describe the evolution of the phase fields $(\sum \xi_j = 1)$:

$$\frac{\partial \xi_j}{\partial t} = -\frac{D}{\alpha} \left[\frac{\delta F}{\delta \xi_j} - \frac{\delta F}{\delta \xi_L} \right], \quad (3)$$

where *j* iterates only over the phase parameters describing the four different solid crystalline orientations. In the equations, *D* is the constant diffusivity of all species in the liquid phase. Finally, Poisson's equation

$$\nabla^2 \phi = -\frac{\rho}{\varepsilon_r \varepsilon_0} \quad (4)$$

must be satisfied everywhere, where ε_r is the relative permittivity, which is assumed to be constant, and ε_0 is the permittivity of free space.

The governing equations (Eqns. 2-4) can be used to predict the electrochemical response of an arbitrary material system under a wide range of environmental conditions based on only a small set of well-defined thermodynamic and kinetic quantities. While precise values of these unknown quantities for Ag in aqueous solution are unknown, we have assigned values that are characteristic of such a system (Table 1). Based on the values provided in Table 1, we have conducted simulations to predict the electrochemical response of this characteristic system. All simulations were conducted on a uniform, two-dimensional grid with mesh spacing of 0.4 Å. A standard explicit finite difference scheme was used to solve Eqns. 2 and 3 with typical time steps on the order of $10^{-13} s$. After each explicit time step a multigrid method was employed to solve

Eqn. 4. Using this approach, the electrochemical response of idealized, small-scale systems with dimensions on the order of 10 nm can be probed over timescales of 0.1 μs to 1.0 μs.

Table 1: Model parameters and their values

parameter	value	parameter	value
T	298 K	$\Delta\mu^{\circ}_{e^-}$	-10.82RT
V_s	10 cm^3/mol	$\Delta\mu^{\circ}_{M^+}$	-10.82RT
W	1.8×10^{4} J/cm^3	$\Delta\mu^{\circ}_{A^-}$	8.70RT
α	1.44×10^{-12} J/cm	$\Delta\mu^{\circ}_{N^+}$	8.70RT
D	1×10^{-5} cm^3/s	$\Delta\mu^{\circ}_{S^0}$	11.45RT
ε_r	80		

Results and Discussion

I. Effect of Substrate Material

Figure 1 shows the concentrations (availability) of Ag^+ ions in 10 microliter droplets of water applied on various material surfaces traditionally used in medical device applications, to re-wet areas where silver nanoparticles were previously deposited and dried. For comparison, the Ag^+ ion concentration in the as-synthesized solution is provided, with an average concentration of 140 mg/L. From this chart two observations may be made. First, the availability of Ag^+ ions is decreased by the process of depositing and drying the nanoparticles onto surfaces. For instance, the highest concentration of available Ag^+ in a reconstituted droplet is on polyethylene (PE) at

approximately 55 mg/L, which is 40% of the level in the as-synthesized solution. Second, the availability of Ag^+ ions differs for the different materials upon which the nanoparticles are deposited, being highest on polyethylene, silicone, and poly(tetrafluoroethylene) (PTFE), and lowest on glass, nitrile rubber, and latex.

The availability of Ag^+ ions after rewetting is affected by the surface charge, chemistry, and wetting properties of the surface. Negatively charged surfaces may bind Ag^+ ions. From Figure 1, the availabilities of Ag^+ ions are highest on polyethylene, silicone, and PTFE, which are charge neutral and chemically inert. In contrast, the availabilities of Ag^+ ions are lowest on glass, nitrile, and latex, which are negatively charged due to electron-rich Lewis-base entities, such as O- at the glass substrate surfaces, the C≡N side groups on nitrile rubber, and the C=C double bond in the latex backbone. For latex, the double bond is not enough to explain the near-complete suppression of the Ag^+ ion availability, since the C=C double bond of latex is a weaker Lewis base compared to the O- surface groups of glass, and yet latex has 2 orders of magnitude lower Ag^+ availability than glass. Closer inspection of the chemical nature of latex reveals it is crosslinked with sulfur, which has a much greater affinity for silver than does O^-. Any sulfur species, whether participating in the crosslinks or residual in the compound can react with and bind Ag^+ ions. Nitrile rubber is also crosslinked with sulfur which also reduces the available Ag^+ ion concentration, but not to complete suppression, as with the latex sample. The difference can be attributed to the extent to which the two samples are crosslinked with sulfur. In fact, the presence of any species with a strong affinity for silver, be it sulfur, chloride, etc., will bind or react with Ag^+, and the amount present will affect the final available Ag^+ ion concentration.

Another observation regarding substrate material is the effect of wettability. During drying of a deposited droplet, the nanoparticles aggregate, agglomerate, and pack together, and

only the exposed surface of the droplet contributes Ag^+ ions into the reconstituting liquid. The higher the wettability of the surface by the aqueous Ag^+ solution, the larger will be the footprint of the deposited droplet. It was observed that of the neutral substrates, the footprints of 10 μL droplets dried on PE, silicone, and PTFE were 7 mm, 4 mm to 5 mm, and 4 mm to 5 mm, respectively, which correspond with the trend of available Ag^+ ion concentration in solution.

From Figure 1 we find that differences exist in available Ag^+ ion depending on the substrate material due to surface charge, chemistry, and wettability. Therefore, any changes in substrate or the substrate surface that cause a change in the surface charge, chemistry, or wettability may impact the antimicrobial effectiveness of applied nanoparticulate silver. These factors should be considered when choosing a material, especially for medical device applications, upon which silver is to be deposited for the purposes of antimicrobial activity.

II. Ion Concentration as a Function of Time.

Figure 2a shows the experimentally derived ion release data of the nanoparticles dried and rewet as a function of time, on three surfaces: polyethylene, glass, and latex. Measurements of ion concentration in the rewet droplet were taken every 5 min. Upon rewetting, surface silver is ionized to Ag^+, giving rise to the increase in ion concentration. In all three cases, ion release increases with time to a maximum value at 5 min into the re-hydration. However, Ag^+ concentration subsequently decreases to undetectable levels (<0.1 mg/L) in approximately 20 min.

Figure 2b shows the predicted ion release versus time curves derived from the continuum model described above, which takes into account the relevant physical, electrical, and chemical contributions to predict the electrochemical response of the silver nanoparticles. Because the

domain size of the simulations (λ_s) is much smaller than the actual experimental system (λ_e), the time scales over which diffusive phenomena are observed are reduced by a factor of $(\lambda_s/\lambda_e)^2$. Thus, for reference the Ag^+ release is also shown as a function of normalized time ($\tilde{t}$) in both Figure 2a (experimental) and 2b (computational), where $\tilde{t}$ =Dt/λ^2 and D is taken to be $1x10^{-5}$ cm^2/s in both cases. The predicted maxima in ion release occur at the same reduced time in both the simulations and experiments. The range of surface charge explored in the simulation was selected to cover the expected range of the substrates used in the experiment. For example, from molecular dynamics calculations we estimate the surface change of latex to be in the range of (2 to 3) $\mu C/cm^2$. Further, we note that the magnitude of M+ release predicted by the model will depend on the particle packing and the specific choice of $\Delta\mu_{M^+}$ used in the calculations, so it is not surprising that we observe discrepancy of about a factor of two between the magnitude of the predicted values for ion release and the experimental data.

With insight from the theoretical model, the observed rise and fall of available ion concentration can be explained by thermodynamic considerations. Due to their high curvatures, the nanoparticles have an initially high Ag^+ solubility and hence a high Ag^+ concentration in solution. However, to reduce the excess surface free energy of the system silver atoms redistribute themselves to coarsen the particles and therefore increase the particles' radii of curvature**.** This coarsening phenomenon is facilitated by the presence of mobile Ag^+ ions in aqueous media, which are dissolved from areas of high curvature and deposited on areas of low curvature. As the surface becomes increasingly smooth, the solubility of Ag+ decreases, thereby reducing the concentration of Ag^+ in solution. As the surface becomes increasingly smooth the additional solubility associated with high curvature structures quickly goes to zero and the solubility becomes equivalent to that in bulk components.

Figure 3a shows a typical TEM micrograph of the silver nanoparticles as prepared and deposited on a lacey carbon-coated copper grid. The synthesis of nanoparticles as described in the experimental section seems to produce two populations of nanoparticle sizes: a smaller, which are approximately 1-2 nm in diameter, and a larger, which range from 6 nm to 20 nm in size. Note that the nanoparticles as prepared are distinct, even when clustered together in agglomerates. Figure 3b shows a typical TEM micrograph of the silver nanoparticles similarly deposited on TEM grids, dried, and subsequently rewet with DI water and re-dried. In the TEM image are several large aggregates of particles formed from smaller nanoparticles coalescing, as can be seen by the smoothing grain boundaries where the particles touch. Even the particles of the originally smaller population have coalesced into larger particles.

The theoretical and computational models give insight into the stability of nanoparticulate systems and indicate that in the presence of aqueous media, which is the case in medical device applications, nanoparticulate silver systems will tend toward restructuring into larger particle surfaces. Figure 4 shows the simulation of the evolution of a nanoparticle coating on a charge-neutral substrate. The simulations predict a coarsening/coalescence of the particles with time of exposure to the solution. As time progresses, the distinct particles simultaneously begin to release metal ions into the solution and coalesce. Simulations also show that substantial electric fields develop at the interface of the coating and solution. As the particles continue to coarsen and reduce their curvature, the amount of metal ions in solution and the magnitude of the electric fields are reduced. These predictions of coalescence, which give rise to the time-dependent ion concentrations seen in Figure 2 are consistent with the TEM observations in Figure 3.

Conclusions

Surface chemistry and reactivity are important considerations in the choice of medical device materials, as they can affect the intended antimicrobial efficacy of applied nanoparticulate silver. Both experimental observations and mesoscale field model calculations show that the substrate upon which silver nanoparticles are deposited affects the ion concentrations of silver, due to surface charge effects, chemical reactivity or affinity of the surface for Ag^+ ions, and wettability of the surface.

Over the course of time, the silver nanoparticles in the presence of aqueous media coarsen to reduce the excess free surface energy of the system. This thermodynamic effect decreases the available concentration of Ag^+ ions and hence the antimicrobial efficacy with time. The required duration of antimicrobial efficacy should also be considered in the design using silver nanoparticle coatings, especially as applied to medical device applications.

FIGURES

Figure 1

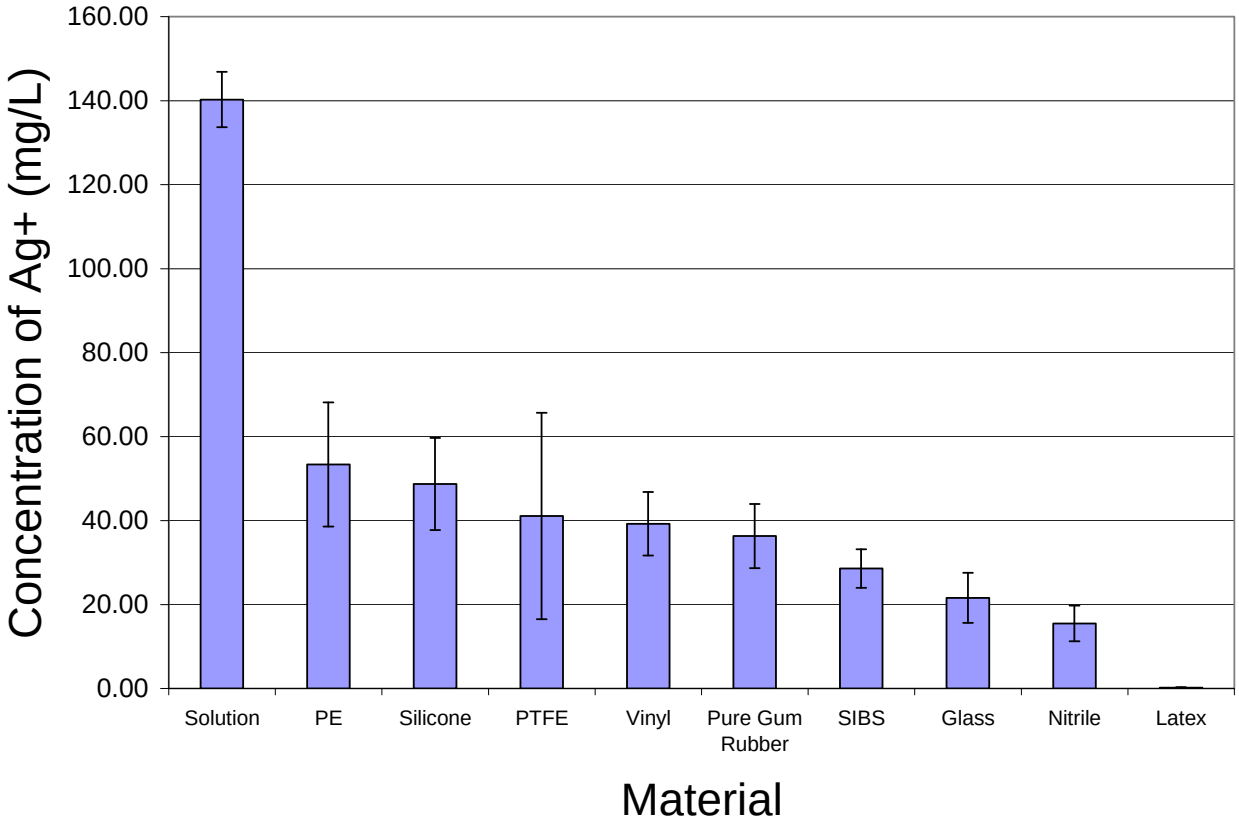

Figure 1: The measured concentration of Ag^{+} ion as a function of material in a droplet of silver nanoparticles, deposited on various substrate materials, dried, and rewet with de-ionized water. Substrates were chosen for relevance to medical device materials: polyethylene (PE), silicone rubber, poly(tetrafluoroethylene) (PTFE), vinyl rubber, pure gum rubber, styrene-b-isobutylen-b-styrene copolymer (SIBS), glass, nitrile, and latex rubber.

Figure 2

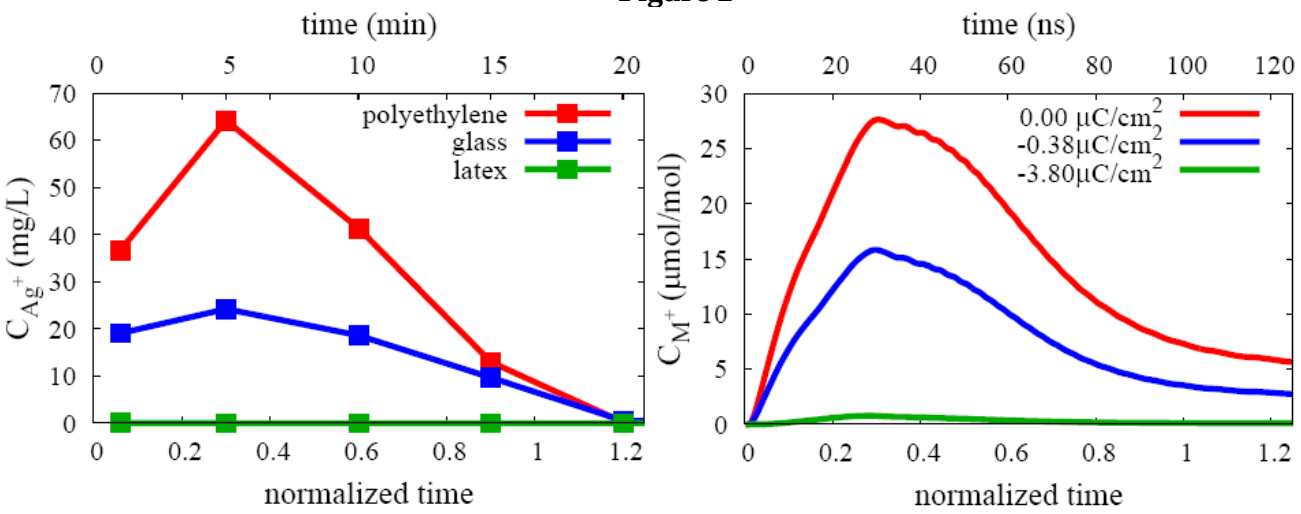

Figure 2a: Measured concentration of Ag^+ ion as a function of time

Figure 2b: Calculated concentration of M^+ ion as a function of time

Figure 3

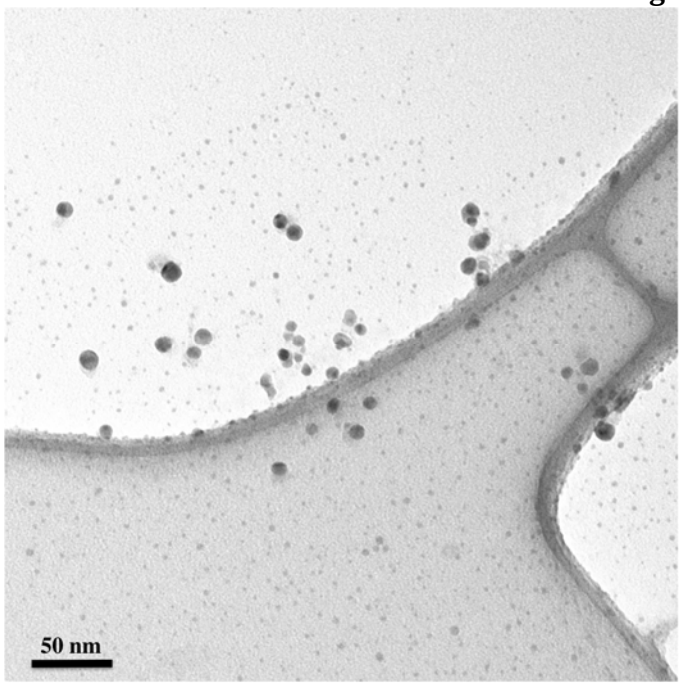

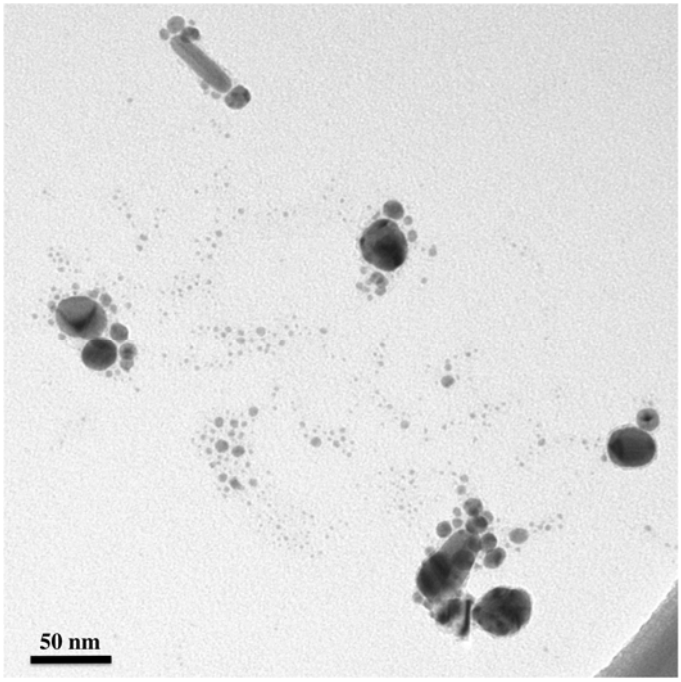

Figure 3a: Transmission Electron Microscope image of as-synthesized silver nanoparticle solution deposited on lacey carbon-coated Cu grids. Particle sizes range from ~6 nm to ~15 nm.

Figure 3b: Transmission Electron Microscope image of silver nanoparticle solution deposited and rewet with DI water. Note the aggregated particles having coarsened surfaces.

Figure 4

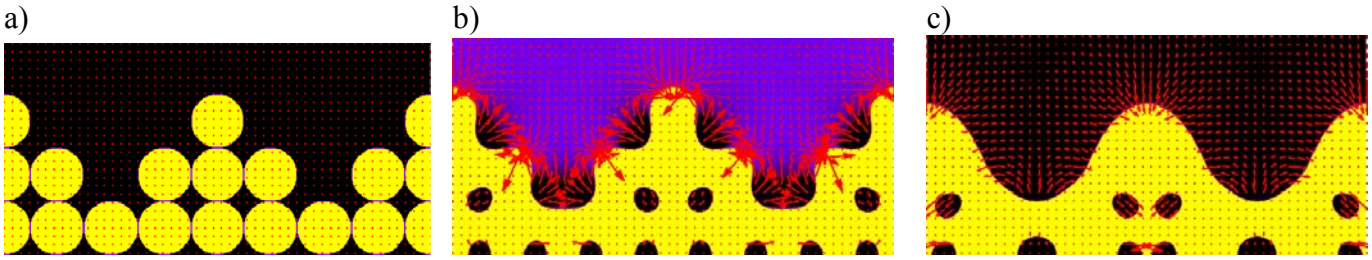

Figure 4: Simulation results showing the evolution of a nanoparticle coating on a charge neutral substrate in a 20 x 10 nm domain. The evolution is shown at normalized time intervals of (a) 0 λ^2/D, (b) 0.25 λ^2/D, and (c) 1.0 λ^2/D. The color in the images varies from black to bright yellow indicating C_{M+} values of $\leq$10 μmol/mol and $\geq$ 1000 μmol/mol, respectively. Also shown in the images are arrows representing the electric field. The direction of the arrows specifies the direction of the field and the length of the arrows is proportional to the magnitude of the field. As time progresses, the 2.5 nm particles that are distinct in the initial coating (a) begin to release M+ ions into solution and coalesce (b). Note that substantial electric fields develop at the interface of the coating and solution. As the particles continue to coarsen and reduce their curvature, the amount of M+ in solution and the magnitude of the electric fields are reduced (c).

REFERENCES

1. White, R. J. An historical overview of the use of silver in wound management. *Br. J. Community Nurs.* **2001**, *6*(8), 3-8.

2. Chen, X.; Schluesener, H. J. Nanosilver: A nanoproduct in medical application. *Toxicol. Lett.* **2008**, *176*(1), 1-12.

3. Wijnhoven, S. W. P; Peijnenburg, W. J. G. M; Herberts, C. A; Hagens, W. I; Oomen, A. G; Heugens, E. H. W; Roszek, B; Bisschops, J; Gosens, I; Meent, D. v. d; Dekkers, S; Jong, W. d; Zijverden, M. v; Sips, A. J. A. M; and Geertsma, R. E. Nano-silver - a review of available data and knowledge gaps in human and environmental risk assessment. *Nanotoxicology* **2009**, *3*(2), 109-138.

4. Lansdown, A. B. G. Silver. I: Its antibacterial properties and mechanism of action. *J. Wound Care* **2002**, *11*(4), 125-130.

5. Chappell, J.B; Greville, G.D. Effect of Silver Ions on Mitochondrial Adenosine Triphosphatase. *Nature* **1954**, *174*, 930-931.

6. Kone, B.C.; Kaleta, M.; Gullans S.R. Silver ion (Ag^+) induced increases in cell membrane K^+ and Na^+ permeability in renal proximal tubule: reversal by thiol reagents. *J. Membr. Biol.* **1988**, *102*, 11-19.

7. Feng, P. L; Wu, J; Chen, G. Q; Cui, F. Z; Kim, T. N; and Kim, J.O; A mechanistic study of the antibacterial effect of silver ions on Escherichia coli and Staphylococcus aureus. *J. Biomed. Mater. Res.* **2000,** *52*(4), 662-8.

8. Lok, C. N; Ho, C. M; Chen, R; He, Q. Y; Yu, W. Y; Sun, H; Tam, P. K; Chiu, J. F; Che, C. M. Silver nanoparticles: partial oxidation and antibacterial activities. *J. Biol. Inorg. Chem.* **2007**, *12*(4) 527-534.

9. Kim, J. S; Kuk, E; Yu, K. N; Kim, J.-H; Park, S. J; Lee, H. J; Kim, S. H; Park, Y. K; Park, Y. H; Hwang, C.-Y; Kim, Y.-K; Lee, Y.-S; Jeong, E. H; Cho, M.-H. Antimicrobial effects of silver nanoparticles. *Nanomedicine* **2007**, *3*(1), 95-101.

10. Jung, W. K; Koo, H. C; Kim, K. W; Shin, S; Kim, S. H.; Park, Y. H. Antibacterial Activity and Mechanism of Action of the Silver Ion in Staphylococcus aureus and Escherichia coli. *Appl. Environ. Microbiol*. **2008**, *74*, 2171-8.

11. Lee, P. C; Meisel, D. Adsorption and Surface-Enhanced Raman of Dyes on Silver and Gold Sols. *J. Phys. Chem.* **1982**, *86*, 3391-5.

12. Certain commercial equipment, instruments, or materials are identified in this paper in order to specify the experimental procedure adequately. Such identification is not intended to imply recommendation or endorsement by either the US Food and Drug Administration or the National Institute of Standards and Technology, nor is it intended to imply that the materials or equipment identified are necessarily the best available for the purpose.

13. Guyer, J. E; Boettinger, W. J; Warren, J. A; McFadden, G. B. Phase field modeling of electrochemistry. I. Equilibrium. *Phys. Rev. E.* **2004**, *69*(2), 021603:1-13.

14. Guyer, J. E; Boettinger, W. J; Warren, J. A; McFadden, G. B. Phase field modeling of electrochemistry. II. Kinetics. *Phys. Rev. E.* **2004**, *69*(2), 021604:1-12.

15. Rappaz, M; Jacot, A; Boettinger, W. J. Last-stage solidification of alloys: Theoretical model of dendrite-arm and grain coalescence. *Met. Mater. Trans. A.* **2003**, *34*(3), 467-479.